Supporting Information

Sansregret et al. 10.1073/pnas.1008403108

SI Experimental Procedures

Cell Culture. Cells were maintained in DMEM (U2OS, NMuMG, NIH 3T3, Rat1, HEK293) or McCoy's media (HCT116 and HCT116 p53$^{-/-}$) supplemented with penicillin/streptomycin, glutamine, and 10% FBS (Gibco). Insulin (10 μg/mL; Sigma) was added for NMuMG cells. Mcf10a were cultured in DMEM/F12 5% FBS, 10 μg/mL insulin, 20 ng/mL EGF, 100 ng/mL choleratoxin, and 0.5 μg/mL hydrocortisone. Stable cell populations were generated with a retrovirus (pREV/TRE vector; Clontech) expressing p110 Cux1 [Myc-(amino acids 747–1505)-HA]. After hygromycin selection for 5 d, more than 500 resistant clones were pooled together, and the population was considered to be at passage 1.

Microscopy. Cells were fixed in 3.7% paraformaldehyde, and stainings were done in blocking solution (PBS, 5% FBS, and 0.5% Triton X-100). Antibodies against γ-tubulin (Sigma T6557), α-tubulin (Abcam ab4074), phospho-histone H3 (Ser28; Cell Signaling #9713) and Centrin 3 (Abcam) were used for indirect immunofluorescence, and secondary detection was done using Alexa-conjugated, species-specific secondary antibodies (Molecular Probes). DNA was stained with DAPI (Sigma). Confocal images were taken using a Zeiss 510 Meta laser scanning confocal microscope (Carl Zeiss) with a 100× objective. Volocity software (PerkinElmer) was used for image analysis.

FACS Analysis and Sorting. For DNA content analysis, cells were fixed in 75% EtOH and stored at −20 °C until analysis. Cells were stained in PBS plus propidium iodide and RNase, then analyzed using a FACScan (Becton Dickinson), using single-cell gating. Cell-cycle profiles were analyzed using FlowJo (Tree Star). Sorting was performed on a MoFlo (Dako) after staining with Hoechst 33342 (2 μg/mL, 1 h).

Antibodies, Western Blot Analysis, Electrophoretic Mobility Shift Assay. pS1237 CUX1 rabbit polyclonal antibodies were generated using the phospho-peptide Cys-YSQGA**pS**PQPQHQ and purified by affinity chromatography (1). CUX1 antibodies (1,300) have been described elsewhere (2). Rabbit anti-p21 and mouse anti-p53 antibodies were a generous gift from Dr. Julian Gannon (Cancer Research UK London Research Institute, London). Electrophoretic mobility shift assay was performed using end-labeled double-stranded oligonucleotides (5′-TCGAGACGATATCGATAAGCTTCTTTTC-3′) as described previously (3).

Western Blot Analysis. Cells lysates were prepared in RIPA-M [10 mM Tris–HCl (pH 8), 1 mM EDTA, 0.5 mM EGTA, 150 mM NaCl, 1% Triton X-100, 0.5% DOC, 0.1% SDS, 1 mM PMSF, protease inhibitor mixture tablet, and PhosStop tablet (Roche)]. SDS/PAGE was performed, and proteins were transferred to PVDF membranes and blocked in Tris-buffered saline-0.1% Tween-20 (TBS 0.1%T) containing 5% milk and 3% BSA. Membranes were probed with antibodies against CUX1 (α-861), pS1237 CUX1, Cyclin B (Lab Vision), or γ-tubulin (Sigma). Primary antibodies were incubated in TBS 0.1%T, and detection was done using an HRP-conjugated α-rabbit or α-mouse secondary antibody in TBS 0.1%T. Immunoreactive proteins were visualized by chemiluminescence with the ECL Western Blotting Detection Kit (Amersham Pharmacia Biotech).

1. Sansregret L, et al. (2010) Hyperphosphorylation by cyclin B/CDK1 in mitosis resets CUX1 DNA binding clock at each cell cycle. *J Biol Chem* 285:32834–32843.
2. Moon NS, et al. (2002) Expression of N-terminally truncated isoforms of CDP/CUX is increased in human uterine leiomyomas. *Int J Cancer* 100:429–432.
3. Santaguida M, et al. (2001) Phosphorylation of the CCAAT displacement protein (CDP)/Cux transcription factor by cyclin A-Cdk1 modulates its DNA binding activity in G(2). *J Biol Chem* 276:45780–45790.

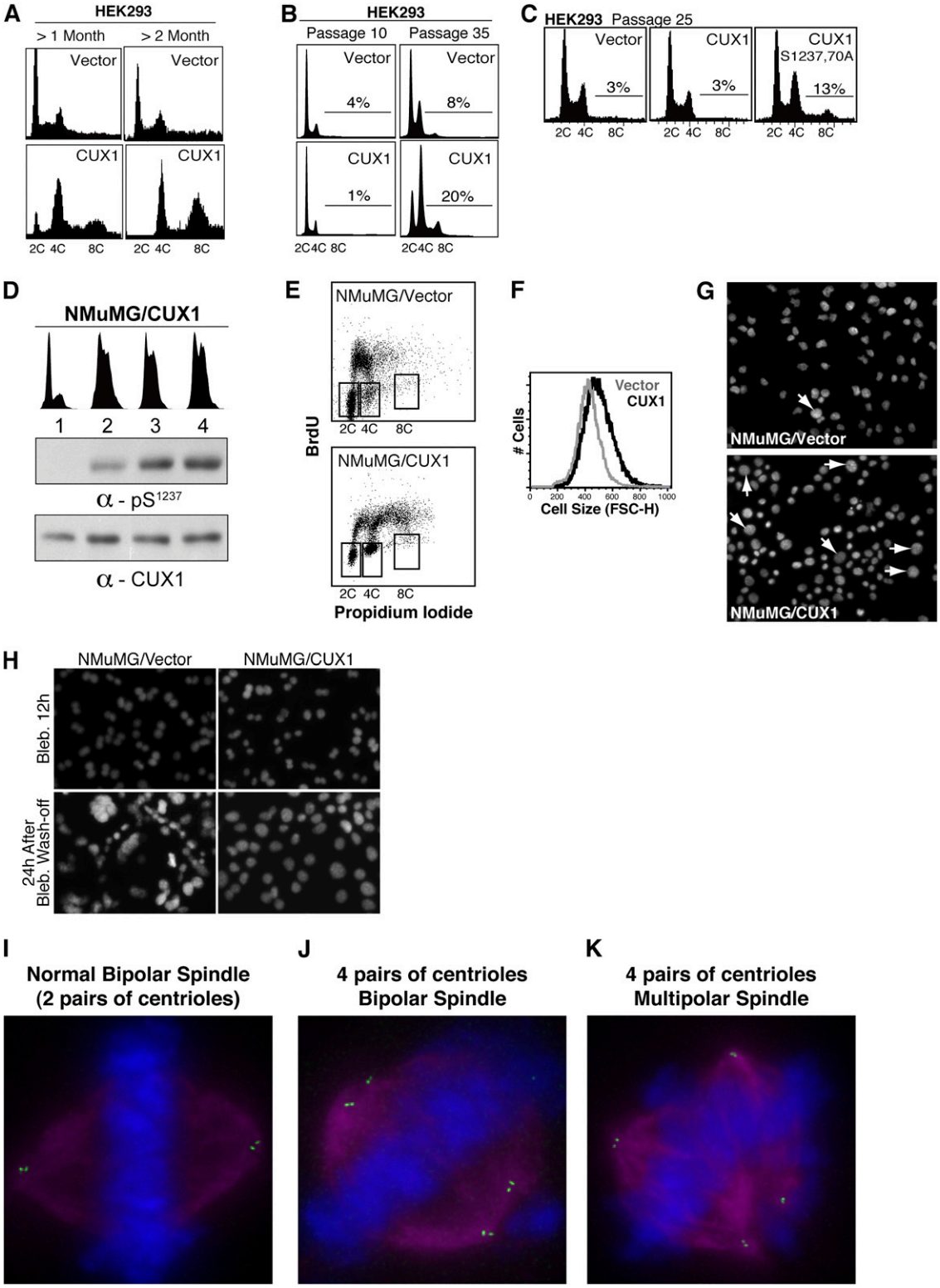

Fig. S1. Characterization of polyploid HEK293 and NMuMG stable cell lines. (*A*) Cell cycle profiles of HEK293/CUX1 or vector controls after more than 2 months in culture, where complete tetraploidization was observed (>2 mo). (*B* and *C*) Cell cycle profiles of independent populations expressing wild-type p110 CUX1 or the $p110^{CUX1S1237,1270A}$ mutant. (*D*) Phosphorylation at serine 1237, which results in inhibition of CUX1 DNA binding, becomes detectable as cells progress in G2. NMuMG cells expressing p110 CUX1 were synchronized in G0 by serum starvation for 3 d and collected after serum restimulation (0 h, 18 h, 19 h, and 20 h). Immunoblotting was performed on whole-cell extracts using purified CUX1-pS^{1237} or CUX1 antibodies using 80 μg and 5 μg of cell lysate, respectively [pS1237-CUX1 antibodies were described previously (1)]. (*E*) Late-passage NMuMG/vector and NMuMG/p110 CUX1 cells were pulse-labeled with 100 μM BrdU for 1 h and fixed in paraformaldehyde for double staining using propidium iodide and an Alexa 649-conjugated anti-BrdU antibody. (*F*) Late passage tetraploid NMuMG/CUX1 are larger as determined by FACS analysis based on forward scatter. (*G*) Late passage NMuMG/CUX1 (unsorted population) contain cells with

Legend continued on following page

various nuclear sizes. Cells were grown on glass coverslips, fixed with paraformaldehyde, and stained with DAPI. (*H*) p110 CUX1 expression prevents the appearance of nuclear abnormalities after blebbistatin-induced binucleation of NMuMG cells. Early-passage cells were treated with 100 μM blebbistatin for 12 h and fixed either after blebbistatin washout (*Upper*) or after an additional 24-h incubation in fresh media (*Lower*). Nuclei were stained with DAPI. (*I–K*) Metaphase spindle configuration in tetraploid U2OS cells with or without MG132. U2OS/vector and U2OS/CUX1 cells were grown on glass coverslips, treated for 8 h with 100 μM blebbistatin, and released for 16 h, after which cells were treated for 1 h with 10 μM MG132 or DMSO and methanol-fixed. Cells were stained with mouse anti-centrin 3 and rat anti-α-tubulin antibodies (followed by species-specific highly crossed-adsorbed secondary antibodies) and DAPI. Metaphase cells were identified according to DAPI staining, and diploid vs. tetraploid U2OS were discriminated on the basis of having two (*I*) or four centriole pairs (*J* and *K*), respectively. Only cells with four pairs were scored in Fig. 2*G* (main text), for which the α-tubulin spindle configuration was determined as being bipolar (*J*) or multipolar (*K*).

1. Sansregret L, et al. (2010) Hyperphosphorylation by cyclin B/CDK1 in mitosis resets CUX1 DNA binding clock at each cell cycle. *J Biol Chem* 285:32834–32843.

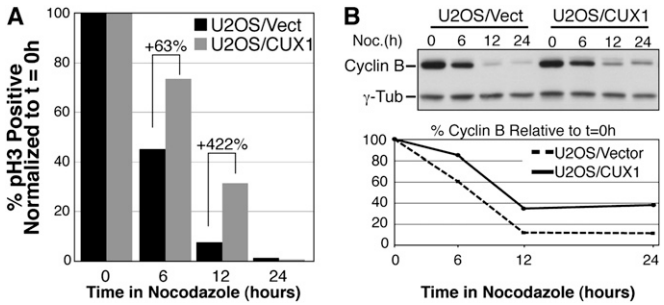

Fig. S2. p110 CUX1 expression allows cells to sustain a longer mitotic arrest and delays cyclin B degradation upon prolonged exposure to nocodazole. (*A*) U2OS/CUX1 and control cells were treated with nocodazole (10 h, 80 ng/mL), after which mitotic floating cells were harvested ($t = 0$ h) and incubated further in the presence of the microtubule poison nocodazole for the indicated times. Cells were fixed and the fraction of mitotic cells determined by FACS according to phospho-histone H3 staining, and normalized to $t = 0$ h for each cell line. Percentage increase vs. vector is indicated. (*B*) Western blot analysis for cyclin B and γ-tubulin was done using cell lysates from Fig. S3*A*. Densitometric analysis was done using ImageJ, and the ratio of cyclin B/γ-tubulin for each time point was expressed as a percentage relative to $t = 0$ h.

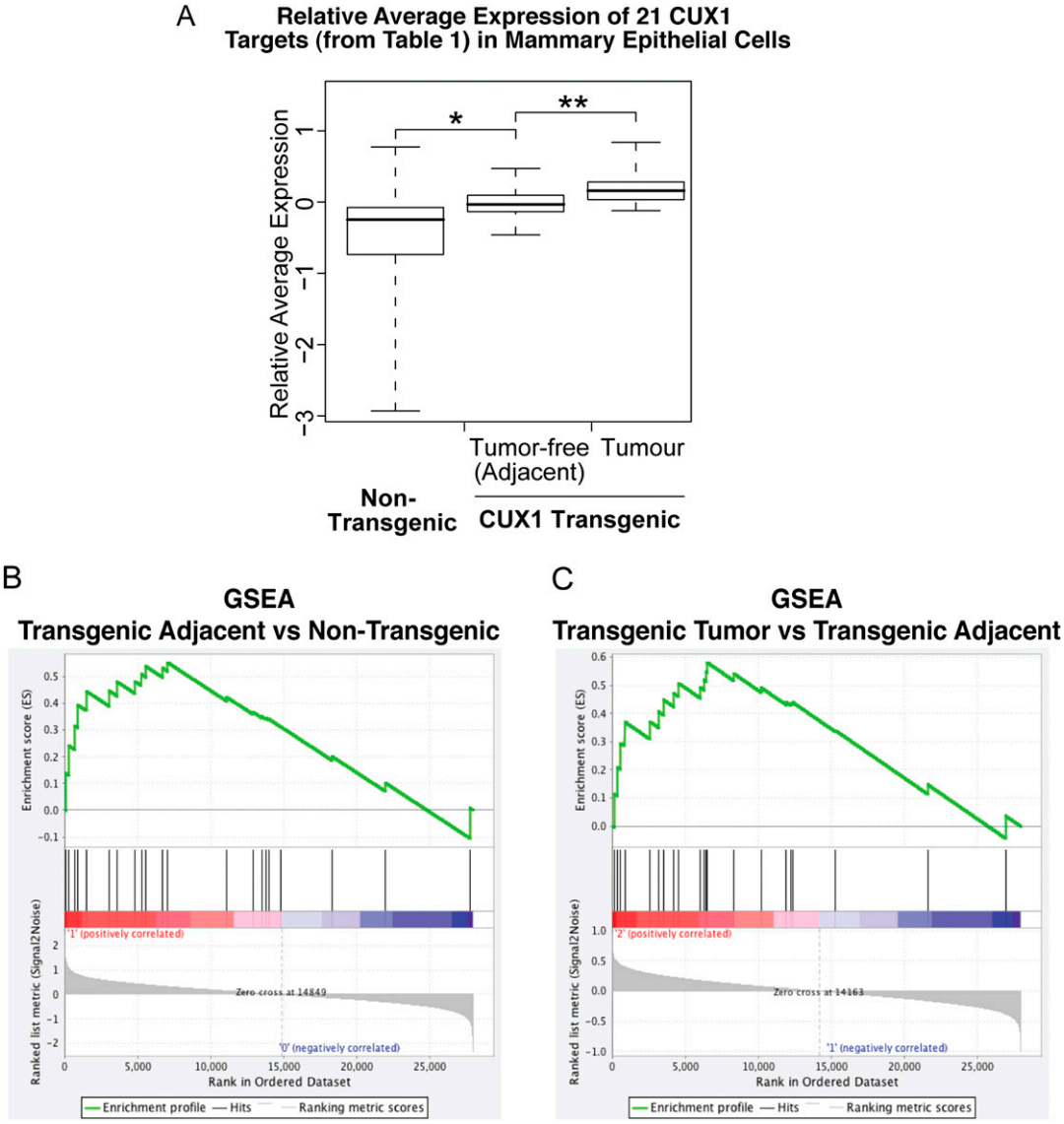

Fig. S3. Expression of 21 CUX1 targets (from Table 1, main text) are cooverexpressed in epithelial cells isolated from mammary tumors of CUX1 transgenic mice. Expression profiling on microdissected epithelial cells was performed using mammary gland tumors or the corresponding tumor-free adjacent mammary gland of CUX1 transgenic mice and normal mammary glands of nontransgenic littermates. (*A*) Distribution of the scaled average gene expression of the CUX1 targets in the three different groups. These graphs show that the overall expression of the CUX1 targets from Table 1 (main text) is higher in tumor-free epithelial cell from CUX1 transgenic mice compared with normal tissue, and even higher in CUX1-driven tumor cells. On average, there was a 1.75-fold increase in the expression of the 21 CUX1 targets in adjacent tissues of transgenic mice compared with normal nontransgenic tissues (*P = 0.014), and a 2.31-fold increase in tumors vs. transgenic adjacent tissues (**P = 0.0016). (*B* and *C*) Gene set enrichment analysis (GSEA). Each vertical line represents one of the CUX1 targets in the signature; the position of the line indicates its enrichment relative to the enrichment of every other gene on the array, with the leftmost position indicating the most enriched gene. The high density of genes at the left of the distribution indicates that the signature as a whole is enriched in this sample. The green line above represents the enrichment score calculated for the signature, and the P value is indicated. GSEA indicated that the 21 CUX1 targets were significantly overexpressed in tissue from CUX1 transgenic mice (*B*, tumor-free CUX1 epithelium vs. normal epithelium, P = 0.0065) and was selected during tumorigenesis in CUX1 transgenic mice (*C*, CUX1 tumor vs. tumor-free CUX1 epithelium, P = 0.0029). Tests were performed using 3,500 gene set permutations on the whole array. Last, a hypergeometric test confirmed that the 21-gene set was significantly overexpressed compared with the entire array (adjacent vs. normal, P = 0.02; tumor vs. adjacent, P = 0.01).

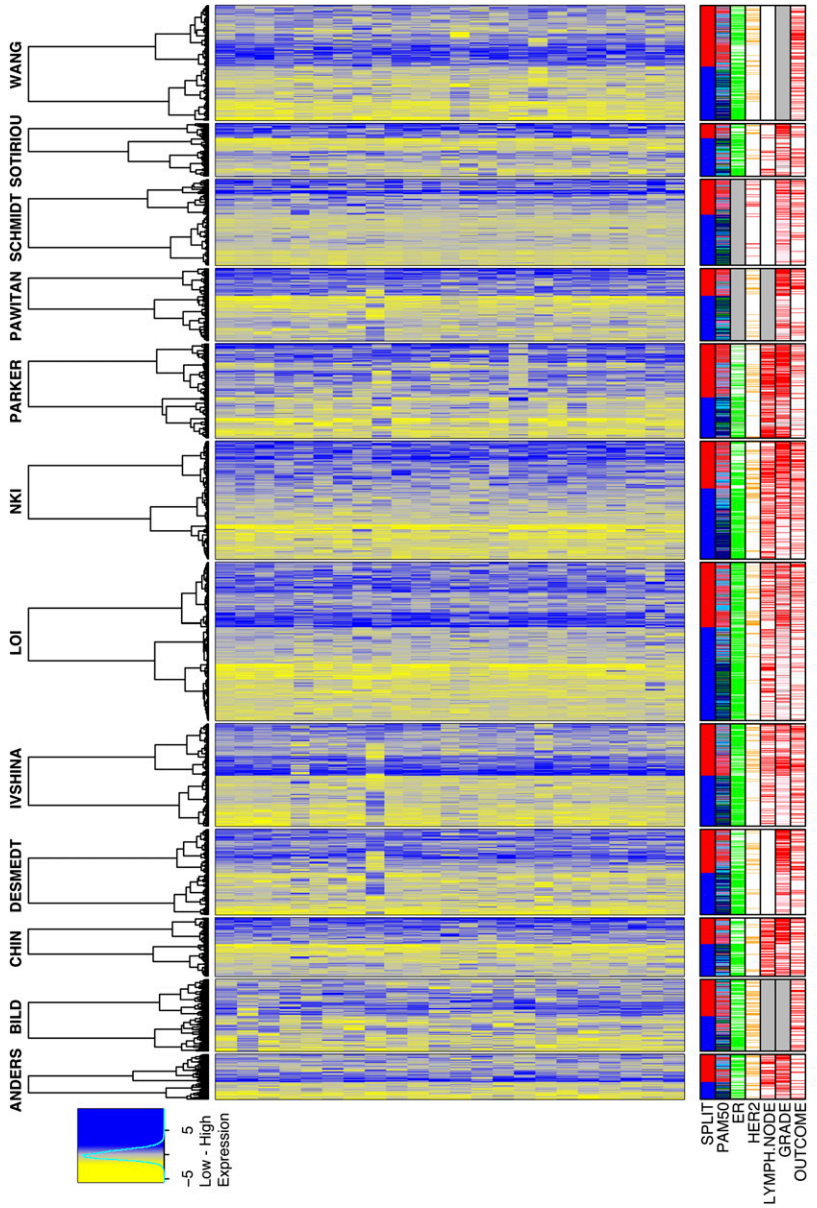

Fig. S4. Euclidean clustering using the 29-gene set within individual datasets. Hierarchical clustering was performed using Euclidean distance and Ward's algorithm. The width of the individual heatmap is based on patient number. Split: blue, low expression of the CUX1 signature; red, high expression. PAM50 (intrinsic subtypes): green, normal-like; dark blue, luminal A; light blue, luminal B; pink, HER2; red, basal. Estrogen receptor (ER): green, estrogen receptor positive (pathology reports); white, ER negative. HER2: yellow, positive (pathology reports); white, negative. Lymph node: red, positive; white, negative. Grade: white, 1; pink, 2; red, 3. Outcome: red, relapse or deceased patient; white, no relapse or survival. Gray, no information available. See refs. 1–12.

1. Anders CK, et al. (2008) Age-specific differences in oncogenic pathway deregulation seen in human breast tumors. *PLoS ONE* 3:e1373.
2. Bild AH, et al. (2006) Oncogenic pathway signatures in human cancers as a guide to targeted therapies. *Nature* 439:353–357.
3. Chin K, et al. (2006) Genomic and transcriptional aberrations linked to breast cancer pathophysiologies. *Cancer Cell* 10:529–541.
4. Desmedt C, et al.; TRANSBIG Consortium (2007) Strong time dependence of the 76-gene prognostic signature for node-negative breast cancer patients in the TRANSBIG multicenter independent validation series. *Clin Cancer Res* 13:3207–3214.
5. Ivshina AV, et al. (2006) Genetic reclassification of histologic grade delineates new clinical subtypes of breast cancer. *Cancer Res* 66:10292–10301.
6. Loi S, et al. (2008) Predicting prognosis using molecular profiling in estrogen receptor-positive breast cancer treated with tamoxifen. *BMC Genomics* 9:239.
7. van de Vijver MJ, et al. (2002) A gene-expression signature as a predictor of survival in breast cancer. *N Engl J Med* 347:1999–2009.
8. Parker JS, et al. (2009) Supervised risk predictor of breast cancer based on intrinsic subtypes. *J Clin Oncol* 27:1160–1167.
9. Pawitan Y, et al. (2005) Gene expression profiling spares early breast cancer patients from adjuvant therapy: Derived and validated in two population-based cohorts. *Breast Cancer Res* 7:R953–R964.
10. Schmidt M, et al. (2008) The humoral immune system has a key prognostic impact in node-negative breast cancer. *Cancer Res* 68:5405–5413.
11. Sotiriou C, et al. (2006) Gene expression profiling in breast cancer: Understanding the molecular basis of histologic grade to improve prognosis. *J Natl Cancer Inst* 98:262–272.
12. Wang Y, et al. (2005) Gene-expression profiles to predict distant metastasis of lymph-node-negative primary breast cancer. *Lancet* 365:671–679.

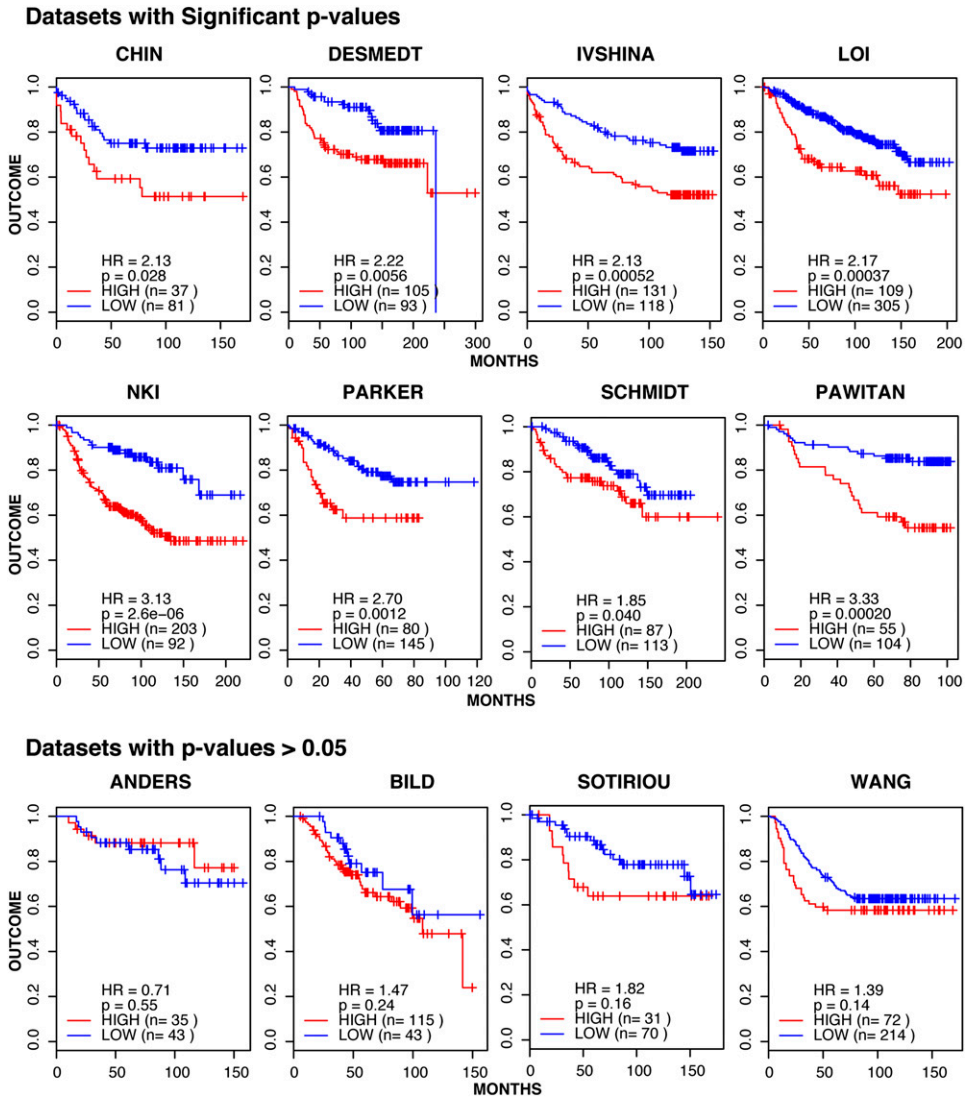

Fig. S5. The 29-gene signature predicts outcome in 8 of 12 datasets. Kaplan-Meier survival analysis and the log–rank test were used to compare the patients in the "low" vs. the "high" classes as determined in Fig. S4. The analysis was completed using the survival package in R/Bioconductor (1).

1. Gentleman RC, et al. (2004) Bioconductor: Open software development for computational biology and bioinformatics. *Genome Biol* 5:R80.

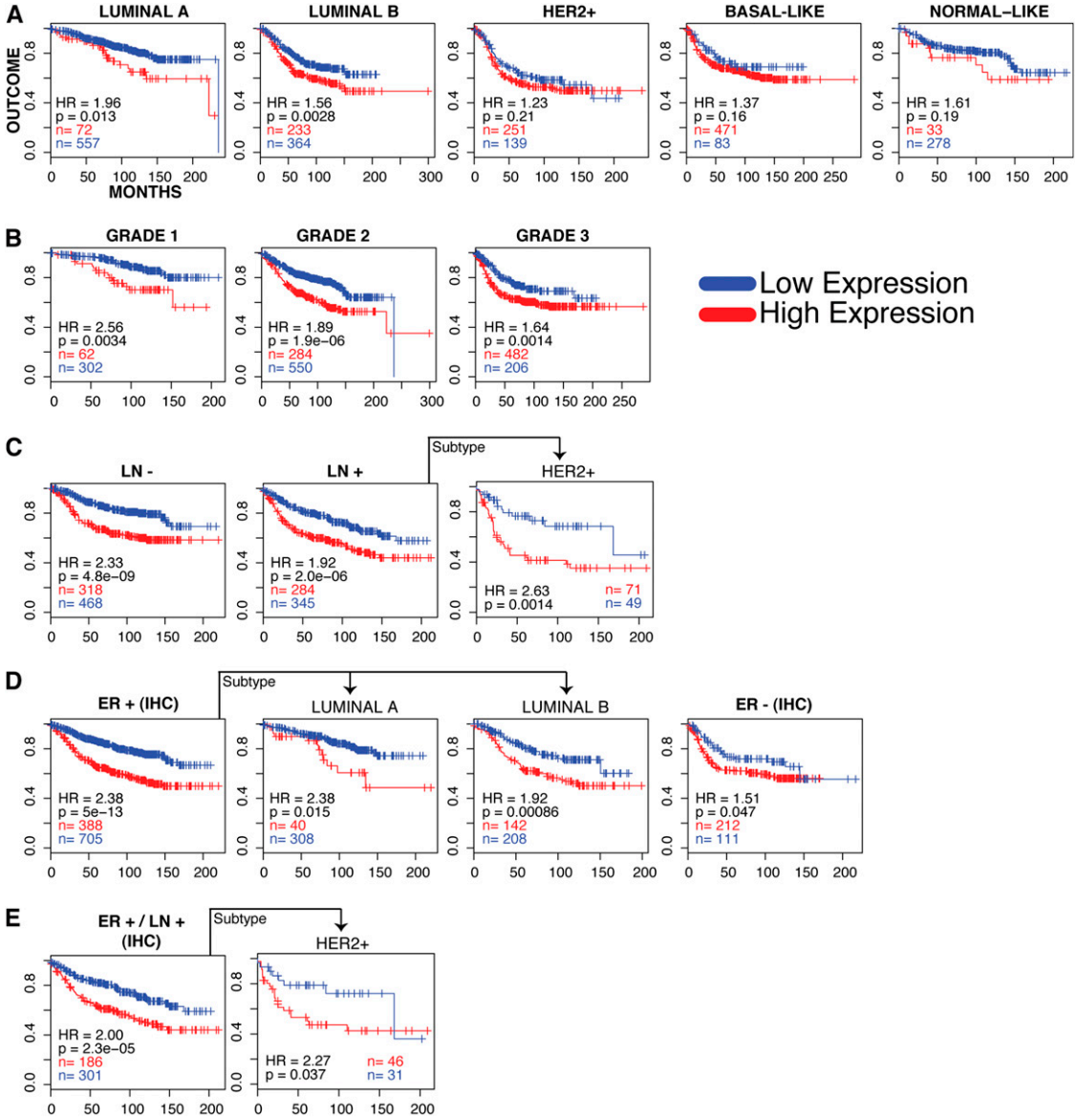

Fig. S6. Predictive value of the 29-gene signature within intrinsic (molecular) subtypes and subgroups with defined clinico-pathological features. Patients from all 12 datasets were combined, and Kaplan-Meier curves show the differential outcome of patients with low or high expression of the CUX1 signature. (*A*) Outcome analysis within intrinsic subtypes defined using the PAM50 classifier. (*B–E*) Information from pathology reports was used to classify patients into subsets of patients (grade, lymph node, or estrogen receptor status). Survival of patient subsets was analyzed according to molecular subtype, and results in which the 29-gene signature showed significant differences in outcome are shown.

Table S1. Cell division followed by time-lapse microscopy

	Vector (late passage)		p110 CUX1 (early passage)		Sorted 8C p110 CUX1 (late passage)	
NMuMG	% Cells	Time in mitosis (min)	% Cells	Time in mitosis (min)	% Cells	Time in mitosis (min)
Bipolar division	99.7	38.6	100	38.5	100	48.0*
Multipolar division	0.3	nd	0	—	0	—

Frequency of bipolar and multipolar division was assessed for late-passage NMuMG/vector (n = 679), early-passage NMuMG/CUX1 (n = 596), and late-passage 8C-sorted NMuMG/CUX1 cells (n = 698). Images were taken every 5 min, and the average time for mitosis was measured (n = 267 for vector; n = 267 for early-passage CUX1 cells; n = 274 for 8C-sorted cells). Mitosis was extended by ≈24% in tetraploid NMuMG/CUX1 cells (48 min) compared with NMuMG/vector cells (38.6 min) or low-passage NMuMG/CUX1 cells (38.5 min). *$P < 0.0001$.

Table S2. Blebbistatin treatment generates binucleated cells

Condition	NMuMG	Mononucleated (%)	Binucleated (%)	Multinucleated (%)
Untreated	Vector (n = 673)	99	1	0
	p110 CUX1 (n = 482)	100	0	0
After blebbistatin	Vector (n = 673)	14	84	2
	p110 CUX1 (n = 482)	11	88	1

Frequency of mononucleated, binucleated or multinucleated cells after 12 h incubation with 100 μM blebbistatin was assessed by microscopy using DAPI staining. The low percentage of multinucleated cells and the low percentage of mononucleated cells suggest that blebbistatin treatment did not encompass more than one doubling time.

Table S3. Primer sequences

Gene	5′–3′	Human genomic	Human cDNA	Mouse cDNA
AurkB	F	GGCAAGGTATGGAGGAAGAGATTTC	CACATTTGACGAGCAGCGAAC	ATCGGGGTGCTCTGCTATGAAC
	R	GGCTCAACAATGTCATCAAGTCC	CACATTGTCTTCCTCCTCAGGG	GTTGCCAGGGGTTATGTTTGAG
Bub1	F	CCCTCCCTTGAGCCAGTAGC	CAAACACATCACTGGGAATGGTTC	TTACATCTGCTGCCCAACTTTCG
	R	TGCCGCATCCCAAACACC	ACAGAGCGTTCTCCAAAGGTCC	ATCGGATAGGTCTTCCACTGTCGC
Bub3	F	GTAGGGAGGCGAGGCGACGGTGTGC	AGGGAGTCCAGCCTGAAATACC	TGACAGACGCAGAAACAAAGCC
	R	CCAGCCCGGCCCACAGCGATG	AAGTGATGCGATGCTCGTGG	TCCCTACCCAAAACAATCACAGG
BUB1B	F	CCCAACACTCAAAACAGCAAAG	TTGGAACACAGGCAGGTCCTTG	GCAGAAACGGGCATTTGAATC
	R	GCAAAACAAATACCCCCAGG	GCTGATGGCTCTGAACCCTTTG	ATCGCTCTCTCCACTAACGCTGAC
Cenpa	F	GCTTTCGGTGACGATTTCAAAC	CTTCCTCCCATCAACACAGTCG	CAGCCGTGGTGTGGATTTTTG
	R	TGGAAGGCAACAGAGTGAGCAG	TGCTTCTGCTGCCTCTTGTAGG	TGGTCAACTGAATGTCTTTGGGG
Cenpe	F	AACGCCGCATCTGATTGAGC	GCTACAATGGTACTATATTTGCCTATGGAC	AGGCTTCAGTGGCTGTCTGTGTTC
	R	ATCCCCTCTCCTGTTTAGCAGTGG	AAGATACACGTAAGAGAAATTCCCTATCAG	TGATGATGGGCACCGCAATC
Mad1L1	F	CCGTAAAGAACCGAGTCTGCGCACC	ACAGGCAGTGTCAGCAGAACTTG	TGGTTGACCTGGAGTTGGAAAAG
	R	GTCCGAGGAGGCTGCCGTGG	TCCCCTTCAGTGCGTTGATG	GCACTGCTGGTGATGCTGTTATTC
Mad2L1	F	GTTTCAAAAGTAACGACGCAGCAC	CGAGTTCTTCTCATTCGGCATC	CAACAGCATTTTGTATCAGCGTGG
	R	ACGACCAGAAGACACATCCTAACC	CCAATCTTTCAGTTGTTCCACCAC	TGGCTTTCTGGGACTTTTCTCTACG
TTK(MPS1)	F	TGGAAGGGCATAAGCAGAAGC	GACTTTCCACCTGCTTGTCAGTTG	ACTTTCCACCTGCCTGTCCATC
	R	TTAGAGAGGATGTGGCAAGAAAGG	CTTGAACCTCCACTTCCTATCTGC	TTGAAGAGGAGTGCTGAGTCCCTG
Nek2	F	GGGCCCTGATCTCGCAGTCTATTGG	TGAAGGAATGCCACAGACGAAG	CGTTTGTTGGCACACCCTATTAC
	R	CCTCTCTCCCGCCCTCCGTTTG	GCACATAACTCATACAGCAAGCAGC	TCCCTTCCCTGATTTTCCCAG
Rod	F	GGGTGGGGCAACTTCCTATTTC	CAGCAGAAAAAAACAGACGAGTTGG	CCTGCTTTTTGTGCTGGATACTG
	R	TCTTCCTGACTCACACAACCGC	GCCAGCACTTTATCAAACATTCGG	TCATCTTCTCCTTCGCTGTTGC
Zw10	F	AAGGAGTGGGTGGAGGAAATAAAC	CAATGGGCGATTCAAAGAAGTC	ATCCGATTGGTCCTGGAAGTG
	R	AAGAGGGAGACTGAAGAGACCAGC	CAAGAAGAGGTTCCAGTCTATGTGC	TGCTGCTGTTTGTGGGAATAGAG
Zwilch	F	AGGTATCTTCTCCCCAACCACTG	CAGGACTTATTGTAGGGGGTGGTC	TTACCTGTTGGGAGAGCAAGGC
	R	CACCCCCTACAATAAGTCCTGTTTG	GAGAAATGGGTCTTTACGGATTCC	AAAGAGGAGGAAGGGCTGTCACTG
Kifc1	F	TGAACCTGTCTCCATCCATCTCTAC	TGAGAAGAAACGGACAAGAGGC	TGACCAAAGTTGACACATCCCGTC
	R	CCTCTTCTCTCAGCCAGCCTACTTAC	TGGACAGGAACAGCAGGAACTG	TTCAGTCTTCTCCCGATAGCGTTTC
Kif2c	F	CCCAGAGCCCTCATTGTCAAATACATAC	TCTCTTCCTTGCTGACTCTCCG	CCCGAAGCAAAAACGCAAATC
	R	CCCAACCATCTTCCTACGCTTG	TCTGCCCATTCCACTGAAACAC	CCTCCTCACTGACCATCAACAACG
Camk2d	F	TCCTGCCTCCTTCCCTAACATC	TCAGAAGAGACTCGTGTGTGGCAC	TGGGGTAAAGGAGTCAACTGAGAGC
	R	GATTACCGCTCACCATCATTCTTC	CATTTGGAATACAGGGTGGCTTG	TGAGCCGAATGTATGCGATGC
Cog7	F	TCGTCTGCCAGGAACTTGGAG	TCATCCAAGAGGTGAACCACGC	TGGTGGATGCTGTGTATGGTCC
	R	TCCCAGCCGCAAACTGAGTG	CCTGAAGAGATTCGGCAGCAAG	TCAATCACTTCCCCGTGTTCC
MFAP(*Mfap1a*)	F	TCCAAACAGTGAACACCAGCAAC	ATGAGGAAATAGAGCGGCGG	TCGGCTCCTTGCTTTTCGTTG
	R	TCCACCATCCCACAATCCTCTC	TTCAATGCTTCGGCTTCACG	CTCCATAGGGGCATAATCTGGTCTC
Nudcd1	F	AAGGAGTAGCAGTGTGGGAGTAAATC	TGCTGCTATTGAGCCTGATGG	GGTGAATCTTGGCAGCAACCAG
	R	TGGAGCATCGCTTGTGAACG	TCTGGAAGCCGTATGGTTACTGTC	TGAATACTCGGCGAAGGCACTC
Rin2	F	ATGTCCTGTTTGTGTCGCTGGCTC	TTTCCAAGAAGAACAAGCAGCG	TCCAACAGGCTCAGCATTCTG
	R	CTTTCCTCATTCATCCCTTCTCG	GATGTAAGGTCTCACAAGGAGGGTC	GGAGGATTTCCGAACCAAAAAG
Sf3b3	F	TCAGCGGAGATTTCGGAGC	CAAGAAACCTTTGGCAAGAGTGG	AAGCGATTCAGCATCCGTCG
	R	AGTTCATTGGGCACTTCTGTGG	GATGAAATGGTAAGTCGGGCTG	CAGTCAACTCTTGGTTACAGCAACG

Primer sequences used to validate the CUX1 transcriptional targets identified by ChIP-on-chip (Table 1, main text), as well as the primers used to analyze their corresponding mRNA levels in mouse and human cells by real-time RT-PCR.

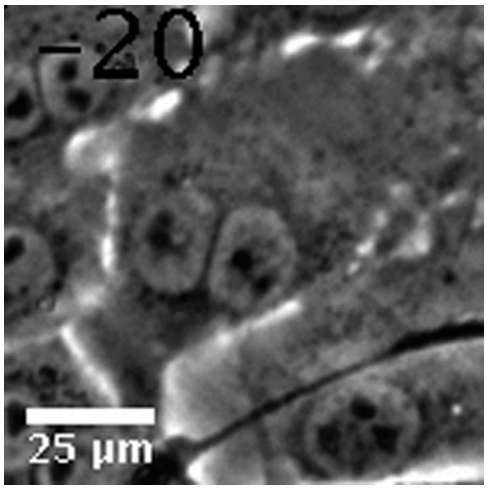

Movie S1. Binucleated NMuMG/vector cell undergoing a tripolar division. Transient (12-h) treatment with 100 μM blebbistatin was used to induce binucleation in early-passage NMuMG cells. Time (in minutes) at which each frame was taken is indicated.

Movie S1

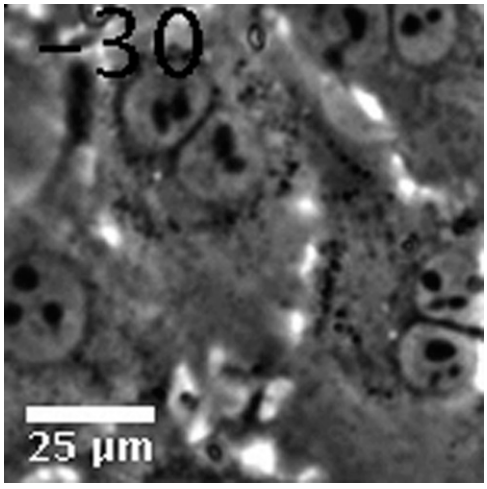

Movie S2. Binucleated NMuMG/vector cell undergoing a tripolar anaphase with incomplete cytokinesis, resulting in one mono- and one binucleated daughter cell. Transient (12-h) treatment with 100 μM blebbistatin was used to induce binucleation in early-passage NMuMG cells. Time (in minutes) at which each frame was taken is indicated.

Movie S2

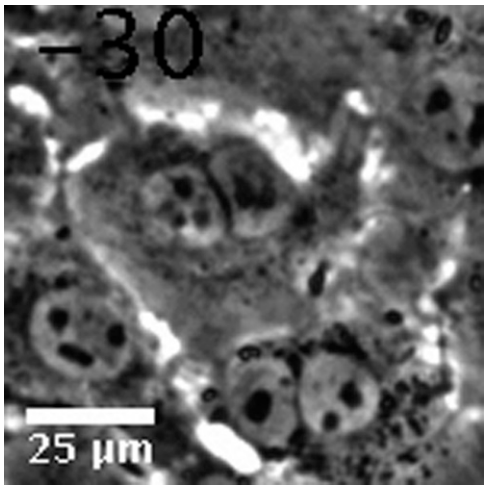

Movie S3. Binucleated NMuMG/CUX1 cell undergoing bipolar division. Transient (12-h) treatment with 100 µM blebbistatin was used to induce binucleation in early-passage NMuMG cells. Time (in minutes) at which each frame was taken is indicated.

Movie S3

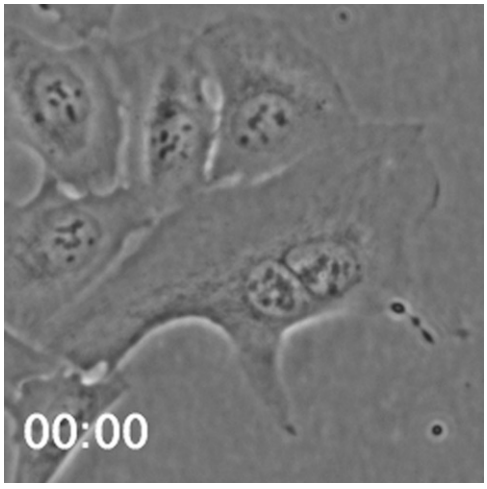

Movie S4. Binucleated U2OS/vector cell undergoing a multipolar division. U2OS/vector cells were treated for 8 h with 100 µM blebbistatin. Sixteen hours after release, cells were followed by time-lapse microscopy, during which 10 µM MG132 was added for 90 min and washed out. We determined the fate of binucleated cells entering mitosis just before or soon after MG132 addition. Neighboring binucleated cells dividing without being exposed to MG132 were used as control.

Movie S4

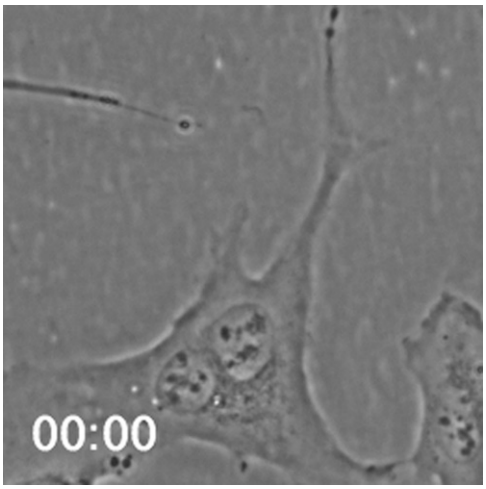

Movie S5. Binucleated U2OS/vector cell undergoing a bipolar division in the presence after transient exposure to 10 μM MG132. U2OS/vector cells were treated for 8 h with 100 μM blebbistatin. Sixteen hours after release, cells were followed by time-lapse microscopy, during which 10 μM MG132 was added for 90 min and washed out. We determined the fate of binucleated cells entering mitosis just before or soon after MG132 addition. Neighboring binucleated cells dividing without being exposed to MG132 were used as control.

Movie S5